The North Atlantic–Eurasian teleconnection in summer and its effects on Eurasian climates

Environmental Research Letters

LETTER

The North Atlantic–Eurasian teleconnection in summer and its effects on Eurasian climates

Jianping Li[1,2,4] and Chengqing Ruan[3]

[1] State Key Laboratory of Earth Surface Processes and Resource Ecology and College of Global Change and Earth System Science, Beijing Normal University, Beijing 100875, People's Republic of China
[2] Laboratory for Regional Oceanography and Numerical Modeling, Qingdao National Laboratory for Marine Science and Technology, Qingdao 266237, People's Republic of China
[3] North China Sea Marine Forecasting Center of State Oceanic Administration, Qingdao 266061, People's Republic of China
[4] Author to whom any correspondence should be addressed.

E-mail: ljp@bnu.edu.cn

OPEN ACCESS

RECEIVED
15 May 2017

REVISED
24 November 2017

ACCEPTED FOR PUBLICATION
24 November 2017

PUBLISHED
30 January 2018

Keywords: Atlantic–Eurasian (AEA) teleconnection, Rossby wave, Eurasian climate, precipitation, surface air temperature

Abstract

A teleconnection between the North Atlantic Ocean and the Eurasian continent is suggested by statistical and dynamical analysis of the northern summer 500 hPa geopotential height field. This teleconnection, termed the Atlantic–Eurasian (AEA) teleconnection, has five centers of action, in the subtropical North Atlantic Ocean, northeastern North Atlantic Ocean, Eastern Europe, the Kara Sea, and north China. The AEA index (AEAI) shows that the AEA undergoes a high degree of variability from year to year, and the AEAI has an increasing trend over the last 30 years. Our results suggest that this phenomenon is a large-scale Rossby wave train that originates in the subtropical North Atlantic Ocean. We support this conclusion by the methods of stationary wave ray tracing in non-uniform horizontal basic flow, wave activity flux calculations, and numerical models. The AEA and midlatitude circumglobal teleconnection pattern manifest distinct features at the hemispheric scale, despite the anomalies associated with them bear some similarities in the northeastern North Atlantic and Eastern Europe. Regional climate variations are strongly linked to this AEA along its path through northern Eurasia.

1. Introduction

The North Atlantic Ocean is a major source of Northern Hemisphere climatic variability (Marshall *et al* 2001, Hurrell *et al* 2002). Fluctuating conditions in both the atmosphere and the ocean in the North Atlantic region have strong climatic effects on surrounding regions, and are also a major source of predictability for climate variability in downstream regions of Eurasia (Hurrell 1995, Benner 1999, Marshall *et al* 2001, Li and Wang 2003b, Ding *et al* 2005, Scaife *et al* 2014, Sun *et al* 2015, Li 2016, Scaife 2016, Sun *et al* 2017). The North Atlantic exerts its climate forcing on remote regions largely through the North Atlantic Oscillation (NAO), which is the leading mode of North Atlantic atmospheric variability in the boreal winter (Walker and Bliss 1932, Bjerknes 1964, Wallace and Gutzler 1981, Li and Wang 2003b, Li *et al* 2013). Many studies have explored the impacts of the winter NAO on temperature and precipitation anomalies in Eurasia and North America (Peng and Mysak 1993, Livingstone 1999, Branstator 2002, Watanabe 2004, Scaife *et al* 2008, Sung *et al* 2010, Xu *et al* 2012, Filippi 2014, Scaife 2016, Yu *et al* 2016, Ding *et al* 2017). In boreal summer, although the NAO is located further north and extends over a smaller area than its winter counterpart (Portis *et al* 2001, Li and Wang 2003b), the teleconnection between the North Atlantic Ocean and Eurasia in the boreal summer is worthy of study.

In fact, the summer NAO (SNAO) can directly exert strong influences on the summer surface climate not only in the northern Europe (Folland *et al* 2009), but also in the Mediterranean region (Bladé *et al* 2012). Bladé *et al* (2012) revealed that the imprint of the SNAO on summer rainfall shows a north–south dipole pattern between northwest Europe and the Mediterranean. Besides the SNAO, there are other modes of large-scale atmospheric variability that can affect European summer climate variability. Ding *et al* (2005) identified a recurrent circumglobal

teleconnection (CGT) pattern in the Northern Hemisphere summertime midlatitude circulation, which was proposed by Branstator (2002) for the boreal winter. Ding *et al* (2005) and Saeed *et al* (2011a, 2011b) have demonstrated that the CGT influences boreal summer regional climates by modulating the Indian summer monsoon. Using both reanalysis data and historical climate simulation of the ECHAM6/MPIOM coupled general circulation model, Saeed *et al* (2014) further investigated the regional impacts of the CGT for the European summer climate at interannual time scales, and demonstrated that through modulating the upper and lower level circulations the CGT is associated with an east–west dipole-like pattern of European summer precipitation, and this relationship is distinct from the SNAO–European summer precipitation relationship (Saeed *et al* 2014).

Wu *et al* (2009) and Wu *et al* (2012) showed that an anomalous NAO in spring can induce a tripole surface temperature anomaly (SSTA) pattern in the North Atlantic Ocean, which persists into the following summer. Zuo *et al* (2012) also found the similar result. The summer tripole SSTA pattern excites a downstream teleconnection in which a distinctive Rossby wave train prevails over northern Eurasia. We term this connection the North Atlantic–Eurasian (AEA) teleconnection, through which the North Atlantic Ocean can affect the climate in East Asia in summer. In this paper, we further investigate the structure of the AEA and explore its mechanism of propagation and regional climate influences.

2. Data and methods

The primary datasets used in this study are the monthly mean 500 hPa geopotential heights, 500 hPa winds, 200 hPa meridional wind, sea surface pressures (SLP), and surface air temperatures from the National Center for Environmental Prediction (NCEP) and the National Center for Atmospheric Research (NCAR) reanalysis datasets (Kalnay *et al* 1996). The monthly rainfall dataset is the Precipitation Reconstruction Dataset (PREC) from the National Oceanic and Atmospheric Administration (Chen *et al* 2002). The period of these datasets is from 1979–2013. In this paper, 'summer' is defined as June–July–August (JJA).

We employ teleconnection (Wallace and Gutzler 1981) and empirical orthogonal function (EOF) analyses to identify teleconnection patterns. We use the stationary wave ray tracing method in horizontally non-uniform basic flow to elucidate the propagation of large-scale Rossby waves (Li and Li 2012, Li *et al* 2015, Zhao *et al* 2015), where the basic flow is the climatological JJA winds at 500 hPa for 1979–2013. We also use the wave activity flux (Plumb 1985) to provide information about the large-scale wave source and sink. Finally, we run a shallow water model, SPMODEL (Hierarchical Spectral Models for Geophysical Fluid Dynamics) (Hayashi *et al* 2003, Takehiro *et al* 2006), to simulate the structure and evolution of the AEA. In the SPMODEL experiment, the basic flow is the JJA 500 hPa wind averaged from 1979–2009, and a source of disturbance is placed in the subtropical North Atlantic (30°N–40°N, 20°W–60°W). The source is centered at (35°N, 35°W), and decreases to zero at the edge. The time step interval of integration is 60 min. After 20 days of integration, the height field become stable. To show the propagation of the AEA wave, we subtract the global average height from the raw data and plot the anomalous height. The CGT index is defined as the first principal component PC1 associated with the leading first EOF (EOF1) of July–August 200 hPa mean meridional wind over the region (100° W–100° E, 20°N–80°N) (Saeed *et al* 2014).

3. Definition and structure of the AEA teleconnection

Figure 1(*a*) shows the map of teleconnections in the Northern Hemisphere JJA 500 hPa geopotential height field. Compared with the winter map (figure 7(*b*) in Wallace and Gutzler (1981)), the strong teleconnection patterns here are located mainly in North America, the North Atlantic, and Eurasia. Fewer teleconnections are located in the North Pacific Ocean, although the western Pacific and Pacific/North American patterns are usually quite strong in winter. In the northern North Atlantic Ocean, a center of action over Greenland is negatively correlated with two centers over eastern North America and the British Isles. This pattern of correlation represents the summer NAO pattern (Li and Wang 2003b, Folland *et al* 2009, Linderholm *et al* 2011). In the eastern North Atlantic, another dipole pattern is found from 30°N–55°N (see the line connecting points A (40°W, 32.5°N) and B (17.5°W, 52.5°N) in figure 1(*a*)), which is similar to the eastern Atlantic pattern in winter in Wallace and Gutzler (1981). In Eurasia, a tripole pattern connects three centers over eastern Baltic Sea (C(25°E, 57.5°N) in figure 1(*a*)), the Kara Sea (D(70°E, 72.5°N) in figure 1(*a*)), and north China (E(107.5°E, 42.5°N) in figure 1(*a*)). This tripole appears similar to the Eurasian pattern in winter in Wallace and Gutzler (1981), but the latitudes of the tripolar nodes in summer are obviously farther north than in winter, and the third center (E in figure 1(*a*)) is located in north China rather than in Japan. Moreover, two other dipole patterns are observed in summer but are absent in winter: the first links the eastern Mediterranean Sea and northern Europe (the ME pattern), and the second links northeast China and the Arabian Sea (the CAS pattern).

Our analysis here focuses on the dipole pattern (A–B) in the eastern North Atlantic and the tripole pattern (C–D–E) across northern Eurasia. The two teleconnection patterns in figure 1(*a*) seem to be separate from

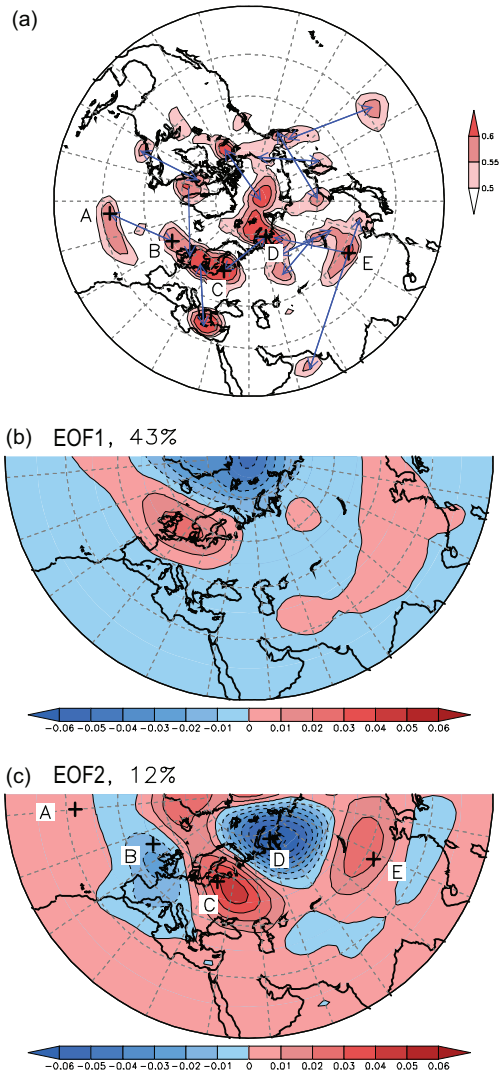

Figure 1. (*a*) Map of teleconnections among 500 hPa geopotential height anomalies in summer in the Northern Hemisphere, for the period 1979–2013. Arrows connect centers of the strongest teleconnections on the one-point correlation map. The crosses denote the five centers of action of the AEA pattern. (*b*) The EOF1 spatial distribution of 500 hPa geopotential height field in JJA over the eastern half of the Northern Hemisphere. The percentage number on the top indicates the explained variance. (*c*) Same as (*b*), but for EOF2. The five crosses are the same as those in (*a*).

each other, but we investigate whether there is some essential connection between them. The teleconnection analysis is a useful tool for diagnosing teleconnections of atmospheric circulation variability; however, the method focuses mainly on oscillations with only two or three centers of action, and may neglect teleconnections with multiple centers. To make up for this weakness, and to find the connection between the North Atlantic and Eurasia, an EOF analysis is applied to the JJA 500 hPa geopotential height field over the eastern half of the Northern Hemisphere (45°W–135°E, 15°N–90°N). The first leading mode (EOF1) is the summer Arctic Oscillation (AO)/NAO pattern, which manifests one sign in the Arctic and the opposite sign in mid-latitudes, with a center over Western Europe (figure 1(*b*)) (Li and Wang 2003a, Folland *et al* 2009, Linderholm *et al* 2011). The second leading mode (EOF2) shows a wave-like pattern (figure 1(*c*)) with five centers of action, located from eastern North Atlantic to northern Eurasia, and is largely consistent with the centers of the dipole and tripole (A–B and C–D–E) teleconnections in figure 1(*a*). This implies a teleconnection structure bridging the North Atlantic and Northern Eurasia in summer, which we term the AEA teleconnection. The AEA index (AEAI) is defined by the geopotential height at the five points:

$$\mathrm{AEAI} = \frac{1}{6}(z'_A + z'_C + z'_E) - \frac{1}{4}(z'_B + z'_D)$$

where z'_P denotes 500 hPa geopotential height anomalies at the point P ($P = A$–E). A positive AEAI is indicative of anomalously high 500 hPa geopotential heights over the subtropical North Atlantic, Eastern Europe, and Mongolia–north China, and low geopotential heights over the northeastern North Atlantic and Kara Sea–northern Siberia; and vice versa.

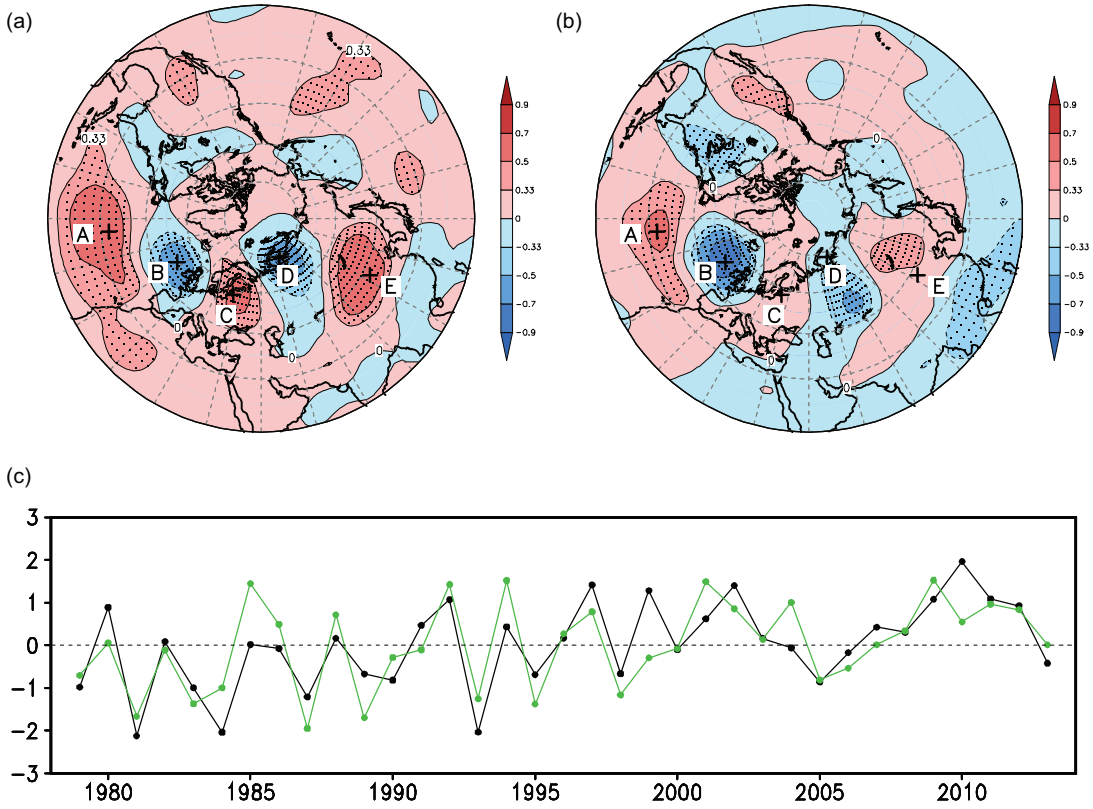

Figure 2. (*a*) Correlation map between the JJA AEAI and Northern Hemisphere 500 hPa geopotential height. The crosses denote the five centers of action of the AEA, and the stippled regions indicate significance at the 95% confidence level using Student's *t*-test. (*b*) Same as (*a*), but for the second principal component (PC2) associated with the EOF2 of 200 hPa meridional wind over (100°W–100°E, 20°N–80°N). (*c*) Normalized time series of the JJA AEAI (black) and the second principal component (green, the average of July and August).

On the correlation map between the summer AEAI and 500 hPa geopotential height (figure 2(*a*)), a wave-like pattern with five nodes is clearly located in the North Atlantic and northern Eurasia, with significant positive correlations in the subtropical North Atlantic, Eastern Europe, and Mongolia–north China, and significant negative correlations in the northeastern North Atlantic and the Kara Sea–northern Siberia. The temporal correlation coefficient between the AEAI and the second principal component (PC2) associated with the EOF2 of 500 hPa geopotential height, mentioned above, is 0.70, while the spatial correlation coefficient between the AEA teleconnection pattern (figure 2(*a*)) and the EOF2 (figure 1(*c*)) is 0.71; both are significant above the 99.9% confidence level. Thus, the AEA resembles the second leading mode of the JJA 500 hPa geopotential height field over the North Atlantic and Eurasia. The time series of the normalized summer AEAI from 1979–2013 in figure 2(*c*) reveals that the AEAI has significant interannual variability, with an increasing trend (the phase shifted from negative to positive AEAI around 1995).

The CGT is an important mode of Northern Hemisphere summer large-scale atmospheric variability in the midlatitudes (Ding *et al* 2005, Saeed *et al* 2011a, 2011b, Saeed *et al* 2014). To what extent does the AEA differ from the CGT? Figure 3 shows schematic illustration of the CGT and AEA teleconnection patterns in summer. The CGT is defined as the EOF1 of JJA Northern Hemisphere 200 hPa meridional wind anomalies (Ding *et al* 2005), and afterwards is extracted over the domain (20°N–80°N, 100°W–100°E) by Saeed *et al* (2011a). The AEA is defined as the EOF2 of JJA 500 hPa geopotential height field over the eastern half of the Northern Hemisphere (45°W–135°E, 15°N–90°N). The CGT has six centers of action from North America–North Atlantic–Eurasia region and shows an east–west mid-latitude wave pattern, whereas the AEA has five centers of action from subtropical North Atlantic–northern Eurasia and its main body spans a larger longitudinal range from subtropical to polar region. The AEA evidently looks more like a southwest–northeast pattern than an east–west wave pattern. Basically, the waves of the AEA originate in the subtropical North Atlantic Ocean (15°W–60°W, 25°N–37.5°N), while those of the CGT originate in the eastern US (70°W–90°W, 35°N–45°N). The wave pathway of the CGT is located in the midlatitudes along the westerly jet, whereas that of the AEA goes to high latitudes from the subtropical North Atlantic Ocean and propagates along the subpolar jet in the high latitudes. The correlation coefficient between the AEAI and CGTI is only 0.15, not significant. However, the correlation maps (figures 2(*a*) and (*b*)) with 500 hPa geopotential

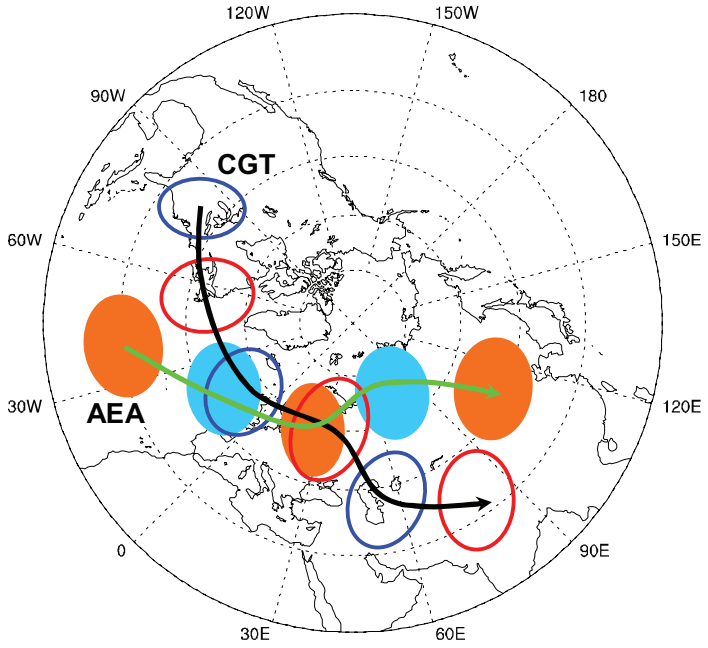

Figure 3. Schematic illustration of the CGT and AEA teleconnection patterns in summer (JJA). The six ellipses denote the six centers of action of the CGT. The shades areas denote the five centers of action of the AEA. The solid black and green curves with arrows denote the wave paths of the CGT and AEA, respectively.

height indicate that AEA is highly related to the EOF2 of 200 hPa meridional wind, and the correlation coefficient between the AEAI and the second principal component (PC2) associated with the EOF2 of 200 hPa meridional wind is 0.75 (figure 2(*c*)), significant at the 99% confidence level. In addition, there are overlaps in the northeastern North Atlantic and Eastern Europe between the CGT and AEA. This implies that there are some overlaps of impacts of the CGT and AEA on summer climate in the northeastern North Atlantic and Eastern Europe (see below). Overall, the difference in the CGT and AEA is essential at the hemispheric scale, though they overlap in the northeastern North Atlantic and Eastern Europe.

4. Propagation mechanisms and the regional climatic influence of the AEA

To demonstrate the characteristics of the propagation of large-scale waves in the AEA pattern, and the path of its influence on downstream regions, we use the wave ray approach of stationary Rossby waves in a non-uniform basic flow, according to Li and Li (2012), Li *et al* (2015), and Zhao *et al* (2015). The wave ray paths in the basic climatological flow at 500 hPa in JJA are mapped in figure 4(*a*), for waves that originate in the subtropical North Atlantic Ocean (15°W–60°W, 25°N–37.5°N) where the first node of the AEA pattern is located. Most of the wave rays that are excited in the source region over the subtropical North Atlantic Ocean propagated along the proposed AEA pathway: first northeast to the British Isles, then east through Europe as far as the Ural Mountains, and finally southeast through Siberia to Lake Baikal, Mongolia, and north China. In addition, a small branch of the rays proceeds southward from Europe to the Mediterranean Sea (this branch might be related to the ME pattern).

The method of wave activity flux gives information on the sources and sinks of waves, and helps us to understand the dynamics of the large-scale Rossby wave (Plumb 1985). Figure 4(*b*) shows composite difference in Plumb's stationary wave activity flux at 500 hPa between the years with a high index (AEAI > 0.5) and the years with a low index (AEAI < -0.5). The wave activity flux is located primarily in the middle latitudes of the North Atlantic Ocean and Eurasia, but also in the subtropical North Atlantic Ocean. In both areas of the North Atlantic, the wave activity flux vectors point northeast, while the flux vectors between 50°N and 70°N in northern Eurasia point east. This indicates that Rossby waves travel from the subtropical North Atlantic Ocean toward the north, then northeast as they crossed the northeastern North Atlantic, Eastern Europe, and Asia as far as Mongolia and north China.

To further analyze the mechanisms of the AEA teleconnection, we employ the SPMODEL (Hayashi *et al* 2003, Takehiro *et al* 2006) in a numerical experiment. A source of disturbance is placed in the subtropical North Atlantic (30°N–40°N, 20°W–60°W), and after 20 days of integration, the height field become stable. It can be seen from figure 4(*c*) that the anomaly height distribution in the SPMODEL simulation is quite similar to the AEA pattern (figure 2(*a*)). Five main centers of anomalous height are located in the subtropical North Atlantic, the northeastern North Atlantic, Eastern Europe, the Kara Sea and north China. This result

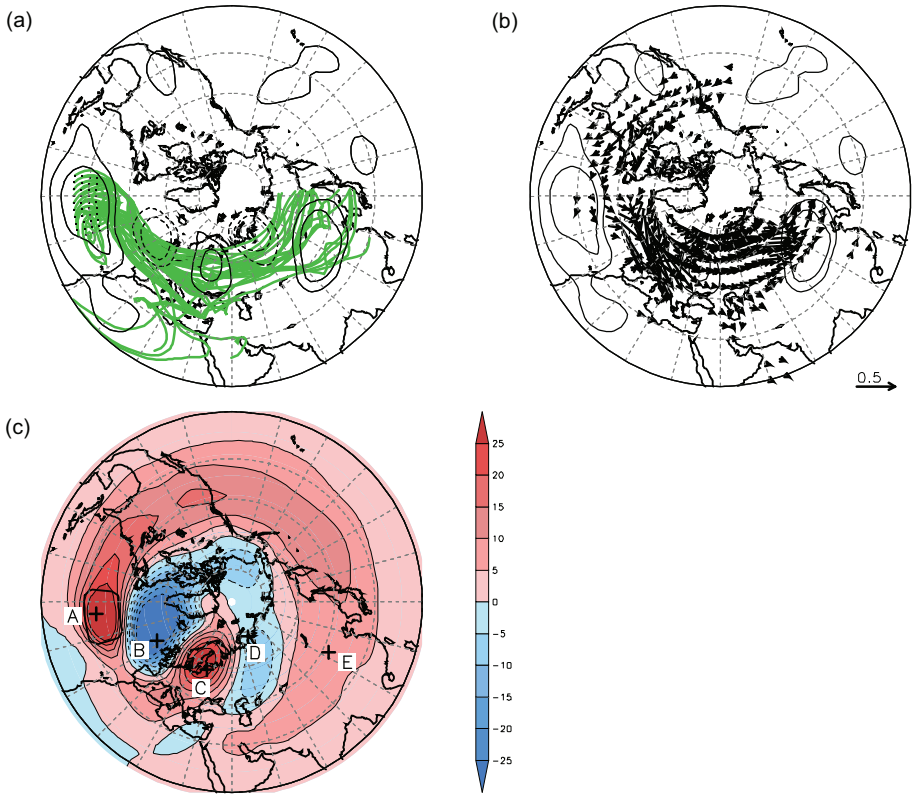

Figure 4. (*a*) Stationary Rossby wave trajectories (green) in the Northern Hemisphere flow in summer at the 500 hPa level. The black dots in the subtropical North Atlantic Ocean mark the wave source region. The black contours represent correlation coefficients of ± 0.33 and ± 0.5, which are correlations between the JJA AEAI and Northern Hemisphere 500 hPa geopotential height. The coefficient value of ± 0.33 is significant at the 95% confidence level using Student's *t*-test. Only rays to the west of 140°E are plotted. (*b*) Composite difference in Plumb's stationary wave activity flux ($m\,s^{-2}$) at 500 hPa between the years of high and low AEAI. The black contours are the same as in (*a*). (*c*) The distribution of anomalous heights on Day 18 from the SPMODEL simulation. Contour intervals are 5 m. The domain enclosed by the thick solid line in the subtropical North Atlantic denotes the region of the disturbance source (30°N–40°N, 20°W–60°W). The crosses denote the five centers of action of the AEA.

further suggests that disturbances in the subtropical North Atlantic Ocean excite a large-scale Rossby wave train that creates the structure of the AEA teleconnection.

Rossby wave propagation in the AEA suggests that the signal in the North Atlantic can propagate to downstream areas, and influence regional climates along the route of the AEA pathway through Europe and north Asia. Figure 5 shows the correlation maps between the detrended AEAI and SLP, precipitation, and surface air temperature in JJA. A five-pole pattern prominently appears in all panels of figure 5, as in the AEA pattern in figure 2(*a*). When the AEAI is positive in summer, significant low SLP anomalies are observed in the northeastern North Atlantic and Europe south of latitude 55°N, and in the Kara Sea and Northern Siberia; and high SLP anomalies are present over Eastern Europe, and Mongolia–north China (figure 5(*a*)). By comparison, the anomalous SLP patterns associated with the CGT (see figure 2(*c*) in Saeed *et al* (2014)) and AEA have obvious different phase, i.e. the 1/4 phase lag between them is observed. Secondly, more precipitation is observed over western and central Europe and northern Siberia, but less over Eastern Europe and Mongolia–north China (figure 5(*b*)). Comparing with the European precipitation anomalies associated with the CGT (figure 8 in Saeed *et al* (2014)), there are some overlaps of impacts of the CGT and AEA on summer precipitation, but there exist some differences. The influence domain of the AEA on summer precipitation in western Europe is further to the south, and that in eastern Europe is further to the north. This indicates that the imprint of the AEA on European summer precipitation displays a southwest–northeast dipole-like pattern, whereas that of the CGT shows an east–west dipole-like pattern (Saeed *et al* 2014). Finally, low temperatures predominate over the northern North Atlantic Ocean, the Kara Sea and northern Siberia, but high temperatures predominate over northeastern Europe and Mongolia–north China (figure 5(*c*)). In comparison with figure 4(*a*) in Saeed *et al* (2014), except the overlap in the northern European region, the significant correlation areas between the AEA and surface air temperature are obvious different from those of the CGT. When the AEAI is negative, the opposite patterns are observed in summer. The relevant indices in the key regions in figure 5(*a*)–(*c*) also exhibit significant correlations with the AEAI in JJA (figure 5(*d*)). The AEAI could account for 31%, 16%, 30% and 18% of the total variance of areal averaged precipitation

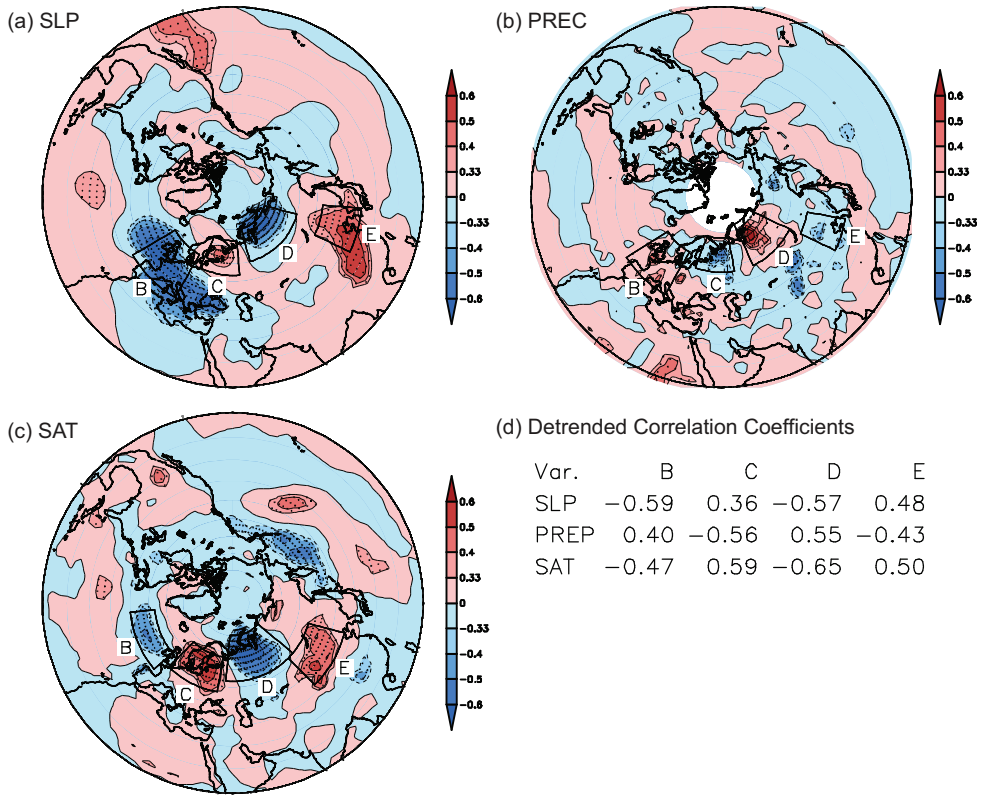

Var.	B	C	D	E
SLP	−0.59	0.36	−0.57	0.48
PREP	0.40	−0.56	0.55	−0.43
SAT	−0.47	0.59	−0.65	0.50

Figure 5. Maps of correlation (detrended) between the JJA AEAI and (*a*) sea level pressure, (*b*) precipitation, and (*c*) surface air temperature. Stippling indicates regions exceeding the 95% confidence level based on Student's *t*-test. The boxes labeled by B, C, D and E in the three panels are key regions with significant correlations. (*d*) Correlations between the JJA AEAI and area-averaged sea level pressure, precipitation and surface air temperature in the boxes B, C, D and E in panels (*a*), (*b*) and (*c*). All values in (*d*) are significant at the 95% confidence level based on Student's *t*-test.

variability over the Eastern Europe, western and central Europe, northern Siberia and Mongolia–north China, respectively. Meanwhile, the AEAI could account for 35%, 22%, 42% and 25% of the total variance of areal averaged surface air temperature variability over northeastern Europe, northern North Atlantic Ocean, the Kara Sea and northern Siberia, and Mongolia–north China, respectively. These results suggest that the AEA teleconnection has strong connections with regional climate variations along the AEA pathway through northern Eurasia.

5. Conclusion and discussion

We find evidence for a new teleconnection pattern, the AEA pattern, in the boreal summer 500 hPa geopotential height field, and document some of its spatial-temporal characteristics. The AEA has five centers of action located in the subtropical North Atlantic Ocean, northeastern North Atlantic Ocean, Eastern Europe, the Kara Sea, and north China. We define an AEAI to depict AEA variations. A positive AEAI is indicative of anomalously high 500 hPa geopotential heights over the subtropical North Atlantic Ocean, Eastern Europe, and Mongolia–north China, and low geopotential heights over the northeastern North Atlantic Ocean and Kara Sea–northern Siberia, and vice versa. The AEA had high year-to-year variability and an increasing trend over the past 30 years. We also compare the differences between the CGT (Ding *et al* 2005; Saeed *et al* 2011a, 2011b, Saeed *et al* 2014) and AEA, and find that the two patterns manifest distinct characteristics (e.g. spatial structure, wave pathway, etc.) at the hemispheric scale, though the anomalies associated with them bear some similarities in the northeastern North Atlantic and Eastern Europe.

The AEA teleconnection is significantly linked with regional climate variations in Europe and north Asia. In the positive phase of the AEAI in summer, less precipitation occurs in Eastern Europe and Mongolia–north China, and more precipitation in western and central Europe and northern Siberia; higher temperatures happen in northeastern Europe and Mongolia–north China, and lower temperatures in the northern North Atlantic Ocean, the Kara Sea and northern Siberia. The opposite occurs with a negative AEAI in summer. We assert that the AEA is a large-scale Rossby wave train originating in the subtropical North Atlantic Ocean. Our conclusion is founded on a stationary wave ray tracing method in non-uniform horizontal basic flow, on the wave activity flux, and on numerical model simulations. We also compare the differences between the imprints of the AEA and CGT on European summer surface climate. There is the 1/4 phase lag between the anomalous SLP patterns associated with the CGT

(Saeed *et al* 2014) and AEA. The CGT is associated with an east–west dipole-like European summer precipitation pattern (Saeed *et al* 2014), while European summer precipitation associated with the AEA displays a southwest–northeast dipole-like pattern. With respect to surface air temperature anomalies associated with the AEA and CGT, except the overlap in the northern European region, the significant anomalous areas are obvious different.

The AEA teleconnection allows a better understanding of links between climate variations in the North Atlantic Ocean and Eurasia. Some associated topics remain to be explored, including the influence of the AEA on regional climates in downstream areas over various space and time scales; other relevant mechanisms including its impacts on the East Asian summer monsoon; and possible links between the AEA and some major climate variations (including the El Nino–Southern Oscillation, the Atlantic Multidecadal Oscillation or Atlantic Multidecadal Variability, the Pacific Decadal Oscillation or Interdecadal Pacific Variability, and the AO/NAO).

Acknowledgments

This work was supported by the National Natural Science Foundation of China (41530424), and the SOA International Cooperation Program on Global Change and Air–Sea Interactions (GASI-IPOVAI-03).

ORCID iDs

Jianping Li https://orcid.org/0000-0003-0625-1575

References

Benner T C 1999 Central England temperatures: long-term variability and teleconnections *Int. J. Climatol.* **19** 391–403

Bjerknes J 1964 Atlantic air-sea interaction *Adv. Geophys.* **10** 1–82

Bladé I, Liebmann B, Fortuny D and Jan van Oldenborgh G 2012 Observed and simulated impacts of the summer NAO in Europe: implications for projected drying in the Mediterranean region *Clim. Dyn.* **39** 709–27

Branstator G 2002 Circumglobal teleconnections, the jet stream waveguide, and the North Atlantic Oscillation *J. Clim.* **15** 1893–1910

Chen M, Xie P, Janowiak J E and Arkin P A 2002 Global land precipitation: a 50 yr monthly analysis based on gauge observations *J. Hydrometeorol.* **3** 249–66

Ding R Q, Li J P, Wang S G and Ren F M 2005 Decadal change of the spring dust storm in northwest China and the associated atmospheric circulation *Geophys. Res. Lett.* **32** L02808

Ding R Q, Li J P, Tseng Y H, Sun C and Zheng F 2017 Linking a sea level pressure anomaly dipole over North America to the central Pacific El Niño *Clim. Dyn.* **49** 1321–39

Filippi L 2014 Multidecadal variations in the relationship between the NAO and winter precipitation in the Hindu-Kush Karakoram *J. Clim.* **27** 7890–7902

Folland C K, Knight J, Linderholm H W, Fereday D, Ineson S and Hurrell J W 2009 The summer North Atlantic Oscillation: past, present, and future *J. Clim.* **22** 1082–1103

Hayashi Y Y, Odaka M, Yamada Y, Morikawa Y, Ishiwatari M, Nakajima K and Takehiro S I 2003 An aqua-planet experiment on structurization of equatorial precipitation activity and related software development toward an Atmospheric General Circulation Model for Terrestrial Planets *CGER's Supercomput. Act. Rep.* **12** 77–86

Hurrell J W 1995 Decadal trends in the North Atlantic Oscillation: regional temperatures and precipitation *Science* **269** 676–9

Hurrell J W, Hoerling M P and Folland C K 2002 Climatic variability over the North Atlantic *Int. Geophys.* **83** 143–51

Kalnay E, Kanamitsu M, Kistler R, Collins W, Deaven D, Gandin L, Iredell M, Saha S, White G and Woollen J 1996 The NCEP/NCAR 40-year reanalysis project *Bull. Am. Meteorol. Soc.* **77** 437–71

Li J P and Wang J 2003a A new North Atlantic Oscillation index and its variability *Adv. Atmos. Sci.* **20** 661–76

Li J P and Wang J 2003b A modified zonal index and its physical sense *Geophys. Res. Lett.* **30** 1632

Li J P, Sun C and Jin F F 2013 NAO implicated as a predictor of Northern Hemisphere mean temperature multidecadal variability *Geophys. Res. Lett.* **40** 5497–5502

Li J P 2016 Impacts of annular modes on extreme climate events over the East Asian monsoon region *Dynamics and Predictability of Large-Scale High-Impact Weather and Climate Events* ed J P Li, R Swinbank, H Volkert and R Grotjahn (Cambridge: Cambridge University Press) pp 343–53

Li Y J and Li J P 2012 Propagation of planetary waves in the horizonal non-uniform basic flow *Chinese J. Geophys.* **55** 361–71

Li Y J, Li J P, Jin F F and Zhao S 2015 Interhemispheric propagation of stationary Rossby waves in a horizontally nonuniform background flow *J. Atmos. Sci.* **72** 3233–56

Linderholm H W, Ou T, Jeong J H, Folland C K, Gong D, Liu H, Liu Y and Chen D 2011 Interannual teleconnections between the summer North Atlantic Oscillation and the East Asian summer monsoon *J. Geophys. Res.* **116** D13107

Livingstone D M 1999 Ice break-up on southern Lake Baikal and its relationship to local and regional air temperatures in Siberia and to the North Atlantic Oscillation *Limnol. Oceanogr.* **44** 1486–97

Marshall J, Kushnir Y, Battisti D, Chang P, Czaja A, Dickson R, Hurrell J, McCartney M, Saravanan R and Visbeck M 2001 North Atlantic climate variability: phenomena, impacts and mechanisms *Int. J. Climatol.* **21** 1863–98

Peng S and Mysak L A 1993 A teleconnection study of interannual sea surface temperature fluctuations in the northern North Atlantic and precipitation and runoff over western Siberia *J. Clim.* **6** 876–85

Plumb R A 1985 On the three-dimensional propagation of stationary waves *J. Atmos. Sci.* **42** 217–29

Portis D H, Walsh J E, El Hamly M and Lamb P J 2001 Seasonality of the North Atlantic Oscillation *J. Clim.* **14** 2069–78

Scaife A A, Folland C K, Alexander L V, Moberg A and Knight J R 2008 European climate extremes and the North Atlantic Oscillation *J. Clim.* **21** 72–83

Scaife A A *et al* 2014 Skillful long-range prediction of European and North American winters *Geophys. Res. Lett.* **41** 2514–9

Scaife A A 2016 The North Atlantic and Arctic Oscillations: Climate variability, extremes and stratosphere troposphere interaction ed J P Li, R Swinbank, H Volkert and R Grotjahn *Dynamics and Predictability of Large-Scale High-Impact Weather and Climate Events* (Cambridge: Cambridge University Press) pp 122–32

Saeed S, Müller W A, Hagemann S and Jacob D 2011a Circumglobal wave train and summer monsoon over northwestern India and Pakistan; the explicit role of the surface heat low *Clim. Dyn.* **37** 1045–60

Saeed S, Müller W A, Hagemann S, Jacob D, Mujumdar M and Krishnan R 2011b Precipitation variability over the South Asian monsoon heat low and associated teleconnections *Geophys. Res. Lett.* **38** L08702

Saeed S, Van Lipzig N, Müller W A, Hagemann S and Jacob D 2014 Influence of the circumglobal wave-train on European summer precipitation *Clim. Dyn.* **43** 503–15

Sun C, Li J P and Zhao S 2015 Remote influence of Atlantic multidecadal variability on Siberian warm season precipitation *Sci. Rep.* **5** 16853

Sun C, Li J P, Ding R Q and Jin Z 2017 Cold season Africa–Asia multidecadal teleconnection pattern and its relation to the Atlantic multidecadal variability *Clim. Dyn.* **48** 3903–18

Sung M K, Lim G H and Kug J S 2010 Phase asymmetric downstream development of the North Atlantic Oscillation and its impact on the East Asian winter monsoon *J. Geophys. Res.* **115** D09105

Takehiro S, Odaka M, Ishioka K, Ishiwatari M and Hayashi Y 2006 SPMODEL: A series of hierarchical spectral models for geophyiscal fluid dynamics *Nagare* **25** 485–6

Walker G and Bliss E 1932 World weather V *Menos R. Meteorol. Soc.* **4** 53–84

Wallace J M and Gutzler D S 1981 Teleconnections in the geopotential height field during the Northern Hemisphere winter *Mon. Wea. Rev.* **109** 784–812

Watanabe M 2004 Asian jet waveguide and a downstream extension of the North Atlantic Oscillation *J. Clim.* **17** 4674–91

Wu Z W, Wang B, Li J P and Jin F-F 2009 An empirical seasonal prediction model of the east Asian summer monsoon using ENSO and NAO *J. Geophys. Res.* **114** D11107

Wu Z W, Li J P, Jiang Z H, He J H and Zhu X 2012 Possible effects of the North Atlantic Oscillation on the strengthening relationship between the East Asian summer monsoon and ENSO *Int. J. Climatol.* **32** 794–800

Xu H L, Li J P, Feng J and Mao J Y 2012 The asymmetric relationship between the winter NAO and precipitation in Southwest China *Acta Meteorologica Sinica* **70** 1276–91

Yu B, Lin H, Wu Z W and Merryfield W J 2016 Relationship between North American winter temperature and large-scale atmospheric circulation anomalies and its decadal variation *Environ. Res. Lett.* **11** 074001

Zhao S, Li J P and Li Y J 2015 Dynamics of an interhemispheric teleconnection across the critical latitude through a southerly duct during boreal winter *J. Clim.* **28** 7437–56

Zuo J Q, Li W J, Ren H L and Chen L J 2012 Change of the relationship between spring NAO and East Asian summer monsoon and its possible mechanism *Chinese J Geophys* **55** 384–95

CORRIGENDUM • **OPEN ACCESS**

Corrigendum: The North Atlantic-Eurasian teleconnection in summer and its effects on Eurasian climates (2018 *Environ. Res. Lett.* 13 024007)

To cite this article: Jianping Li and Chengqing Ruan 2018 *Environ. Res. Lett.* **13** 129501

Environmental Research Letters

CORRIGENDUM

Corrigendum: The North Atlantic-Eurasian teleconnection in summer and its effects on Eurasian climates (2018 *Environ. Res. Lett.* 13 024007)

Jianping Li[1,2] **and Chengqing Ruan**[3]

[1] State Key Laboratory of Earth Surface Processes and Resource Ecology and College of Global Change and Earth System Science, Beijing Normal University, Beijing 100875, People's Republic of China
[2] Laboratory for Regional Oceanography and Numerical Modeling, Qingdao National Laboratory for Marine Science and Technology, Qingdao 266237, People's Republic of China
[3] North China Sea Marine Forecasting Center of State Oceanic Administration, Qingdao 266061, People's Republic of China

E-mail: ljp@bnu.edu.cn

OPEN ACCESS

RECEIVED
24 October 2018

ACCEPTED FOR PUBLICATION
25 October 2018

PUBLISHED
7 December 2018

In the published paper, one reference was left out and wrongly cited. The missing reference is 'Ding and Wang 2005 Circumglobal teleconnection in the northern hemisphere summer *J. Clim.* **18** 3483–3505'. It was wrongly cited in three places:

(1) The second paragraph in 1. Introduction: … 'Ding *et al* (2005) identified a recurrent circumglobal teleconnection (CGT) pattern …'

(2) The second paragraph in 1. Introduction: … 'Ding *et al* (2005) and Saeed *et al* (2011a, 2011b) have demonstrated that the CGT …'

(3) The fourth paragraph in 3. Definition and structure of the AEA teleconnection: … '200 hPa meridional wind anomalies (Ding *et al* 2005), and afterwards …'

In these three places, 'Ding *et al* (2005)' or 'Ding *et al* 2005' should be 'Ding and Wang (2005)' or 'Ding and Wang 2005'.

ORCID iDs

Jianping Li https://orcid.org/0000-0003-0625-1575

References

Ding Q and Wang B 2005 Circumglobal teleconnection in the northern hemisphere summer *J. Clim.* **18** 3483–505